IEEE Access
Multidisciplinary | Rapid Review | Open Access Journal

Date of publication xxxx 00, 0000, date of current version xxxx 00, 0000.

Digital Object Identifier 10.1109/ACCESS.2017.DOI

Frequency Scanning Single-ridge Serpentine Dual-Slot-Waveguide Array Antenna

WEISHUANG YIN[1], (Student Member, IEEE),ANG CHEN[1],XIUYE LIANG[1], (Student Member, IEEE),LEI SHI[1],FANG GUAN[1,2], XIAOHAN LIU[1], AND JIAN ZI .[1]

[1]Department of Physics, Fudan University, 2005 Songhu Rd ShangHai 200438, China (e-mail: wsyin14@fudan.edu.cn; achen12@fudan.edu.cn; xyliang16@fudan.edu.cn;lshi@fudan.edu.cn; fguan@fudan.edu.cn; liuxh@fudan.edu.cn; jzi@fudan.edu.cn)

[2]Institute for Nanoelectronic devices and Quantum computing, Fudan University, Shanghai 200438, China. (e-mail: fguan@fudan.edu.cn)

Corresponding author: Fang Guan (e-mail: fguan@fudan.edu.cn).

This work was supported in part by 973 Program and China National Key Basic Research Program (2015CB659400, 2016YFA0301103, 2016YFA0302000 and 2018YFA0306201) and in part by National Natural Science Foundation of China (11774063, 11727811, 91750102 and 11604355).

ABSTRACT This paper presents a novel one-dimensional (1D) frequency scanning dual-slot-waveguide array antenna with versatile advantages such as large scan volume, high frequency sensitivity, low cross-polarization and low sidelobe. Electromagnetic waves radiate through the leaky-wave dual slots, machined on the side chambers of the single-ridge serpentine waveguide. By properly designing the serpentine waveguide, which plays the role of delay line, such 1D frequency scanning array antenna can achieve 39° scanning over a frequency range from 9.7 GHz to 10.3 GHz, and high frequency sensitivity of 65°/GHz. The dual slots with all the adjacent monomers inclined in same direction are designed to acquire low cross-polarization and avoid high-order mode radiation. The cross-polarization is 45 dB lower than the corresponding co-polarization over the whole working band. Taylor aperture distribution is employed to achieve a low sidelobe (−21 dB). The nonresonance VSWR is below 1.2, and meanwhile the resonance VSWR remains a low level, around 2.5. Furthermore, our proposed 1D array as a building block can compose a novel 2D electric scanning array, with frequency scanning in one dimension and phase scanning in the orthogonal dimension. A 2D array consisting of three waveguide elements is simulated to predict the phase scanning performance, and the results indicate that a 120° scanning performance can be obtained. At last, a 1D serpentine dual-slot-waveguide array antenna is fabricated, whose measurements show good agreement with simulations.

INDEX TERMS Single-ridge waveguide, dual slots, frequency scanning, phase scanning.

I. INTRODUCTION

ELECTRONIC scanning antennas are widely used in modern radar and communication systems for their controllable beams. Two-dimensional (2D) active phased array antenna with flexible programming capabilities has emerged as a fundamental technology to realize the beam scanning over the years [1]–[3]. However, they are usually costly due to the requirement for large number of transmitting and receiving (TR) components, thus limiting the scope of their applications. The frequency scanning array (FSA) that supports an efficient and economical way to realize beam-scanning capabilities through tuning the frequency, is a good compromise proposal, which can be used in many specific scenarios. Because of eliminating complex feeding network, the FSA is also easier to be fabricated [4], [5].

The research of FSAs dates back to the 1940s, which can be classified into two categories, one is linear array series fed by the slow-wave structure, and the other is leaky-wave antennas (LWAs) [6]. For the first type, the equivalent propagation constant can vary with the length of the meandering slow-wave line. Such FSA can scan from backfire to endfire with high frequency sensitivity, which means the beam angle scans quickly with less frequency resources. The metal waveguide is often used for implementing frequency scanning due to its simple structure and low loss [7]–[9]. R. S. Elliott has reported an edge slot FSA based on a snaked

This article has been accepted for publication in a future issue of this journal, but has not been fully edited. Content may change prior to final publication. Citation information: DOI 10.1109/ACCESS.2020.2989318, IEEE Access

X-band rectangular waveguide [10], which can scan the beam from 69° to 102° over 6% frequency band. However, it is bulky and can not form a large 2D electric scanning array. Then with the development of patch antennas, a lot of research has been done on frequency scanning microstrip antennas [11], [12]. A microstrip FSA for imaging applications is proposed in [13], where the radiating patches are feed by a main delay line. A 50° scanning range is obtained with a frequency sensitivity of 11.67°/GHz. The printed FSAs have the advantages of low profile, small volume, light weight and convenient processing. However, the gain and efficiency are quite low due to the losses of the microstrip line.

As a member of traveling-wave antennas, LWA has also been intensively investigated due to its frequency scanning capability and simple feeding network. The uniform LWA whose dominant mode is a fast wave that therefore radiates whenever the structure is open. The most common example of such an antenna is a rectangular waveguide with a continuous slit cut along its side [14]. While the radiation from this type of LWA is limited to the forward quadrant. The second type of LWA is periodic LWA, in which some periodic modulation of the guiding structure is introduced, and -1 order mode is used most frequently for leaky-wave radiation. Microstrip line [15] and waveguide [16] are the common used guiding structures. Reference [17] proposed a low-profile FSA based on substrate integrated waveguide (SIW), which achieved a wide scanning range of -30° $\sim$ 30° and a maximum gain of 10 dB. The SIW technology provides a reasonable tradeoff between the dielectric-filled metallic waveguide and microstrip technologies, which have the advantages of relatively low loss, low profile and ease in integration. Composite right/left-handed (CRLH) metamaterial based LWAs have been a research hotspot over the past decades due to their backfire to endfire scanning ability, including the broadside direction [18]–[20]. By using the balanced transmission line, the open-stopband problem [21] usually occurred in the periodic LWAs has been overcome. However, the aperture distribution of this type of LWA is difficult to control, thus usually leading to high sidelobe level in the radiation patterns. In addition, due to the small changes of the propagation constant, wideband frequency resources are usually required to achieve large scanning angles.

The ridge gap waveguide (RGW) is considered a new technology to build different kinds of microwave components [22], [23]. A LWA based on RGW with nonresonant slots is first constructed with a scanning capability of 17° [24]. However, except the small scanning angle, it suffer from undesirable grating lobes. A split slots array in RGW is proposed to suppress the grating lobes, while the radiation beam can only scan in one side of the boresight [25]. In addition, the width of the RGW is more than half of a wavelength, thus the grating lobe will appear when building a 2D array. The strengths of the RGW technology are its low loss and high-power handing ability with minimal complexity by avoiding any kind of waveguide connectivity. It's a very competitive choice for high frequency applications, especially for millimeter wave band, while may not be necessary at low frequency when compared with the simple rectangular waveguide.

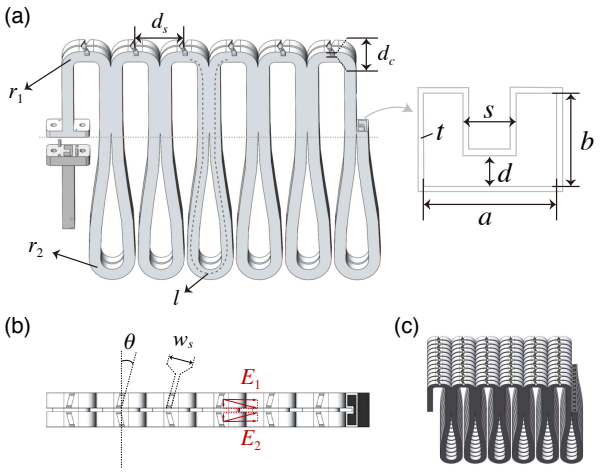

FIGURE 1. (a) Schematic view of an SSDA with six dual slots, with the top-right inset showing the cross section of the waveguide. The structure parameters are labeled aside. (b) Top view of the structure, with the inclined angle θ and width of the slot w_s. Electric fields $E_{1,2}$ are perpendicular to the corresponding slots, respectively. (c) A 2D array composed of six stacked SSDAs.

In this paper, we cast our eyes on the air-filled metal waveguide. Its advantages of low loss, good stability and reliability, and high power handling capability are highly valued for many specific outdoor applications, such as airfield control radar and harbor surveillance control radar. Thus we propose a novel one-dimensional (1D) frequency scanning dual-slot-waveguide array antenna. The slow-wave structure as well as the radiating elements are studied comprehensively to obatian large scan sector, high frequency sensitivity, low cross-polarization and low sidelobe level (SLL). The radiating elements, consisting of two inclined slots, directly located on side chambers of the serpentine waveguide. The radiating slots have different tilting angles, forming desired aperture distribution. The feed network involved here is that all the slots are excited by the single-ridge serpentine waveguide. As a slow-wave structure, the serpentine waveguide provides expected phase delay to the slots, which radiate electromagnetic fields by cutting the currents in the waveguide. Such 1D array antenna can work alone, or as a subarray element to compose a 2D array via putting tens of waveguides together. The 2D array can scan in frequency along the waveguide, while scan in phase along the perpendicular direction with phase shifters. When applied to the previously mentioned scenarios, such 2D array can be installed on the radar tower.

This paper is organized as follows. Section II shows the design of single-ridge serpentine dual-slot-waveguide array (SSDA) in detail, including the serpentine waveguide, dual slots and array design. Section III presents the simulation and analysis results. Section IV demonstrates the fabrication of prototype array and the measurement results. Finally,

This article has been accepted for publication in a future issue of this journal, but has not been fully edited. Content may change prior to final publication. Citation information: DOI 10.1109/ACCESS.2020.2989318, IEEE Access

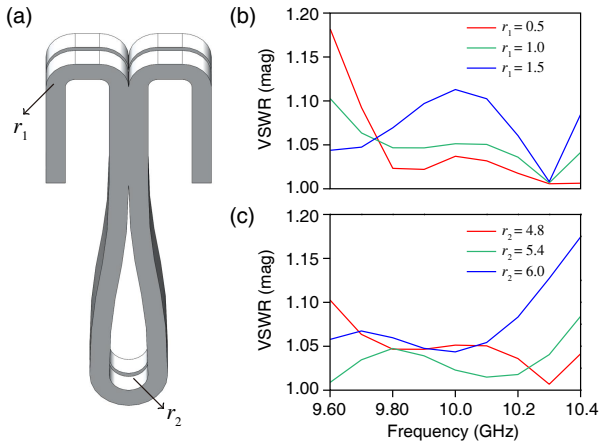

FIGURE 2. (a) Structure chart of the unit for single-ridge serpentine waveguide with two key parameters r_1 and r_2. (b) VSWR of the unit with different r_1. (b) VSWR of the unit with different r_2.

conclusions are drawn in V.

II. ANTENNA STRUCTURE AND DESIGN

The configuration of the frequency scanning SSDA is illustrated in Fig. 1(a), which is composed of six dual-slots. The radiating slots on the waveguide are an integral part of the feed system, which is the waveguide itself. When the slots are cut into a waveguide wall and it interrupts the flow of current, power is coupled from the waveguide modal field through the opening to free space. This antenna is fed by a connector through a waveguide coaxial junction on the left, and terminated by a matched load on the right to eliminate reflection (not shown). Fig. 1(b) is the top view of the SSDA, all the dual slots are inclined in the same direction, while monomers within the dual slots incline oppositely towards the perpendicular direction of the waveguide line. A 2D array is shown in Fig. 1(c), composed of six stacked SSDAs, which can realize frequency and phase hybrid electronically scanning. With that configuration, the azimuth plane is scanned by frequency, while the elevation plane scanned by phase using phase shifters. And the top-right inset of Fig. 1 gives the zoomed view of the waveguide cross-section.

A. SINGLE-RIDGE WAVEGUIDE DESIGN

The SSDA can be divided into two parts by the horizonal dotted line in Fig. 1(a). Within the two parts, the radius (r_1) of the upper transition is small, while that (r_2) of the lower transition is larger. In order to leave more space between the radiation slots and the waveguide transition, we make the radius r_1 small, giving enough length to attenuate high-order modes; the large radius r_2 is aimed at reducing the reflection and also maximizing the space usage.

Meanwhile, the radii r_1 and r_2 are key parameters for reflection performance of the single-ridge serpentine waveguide. Fig. 2(a) plots the structure chart of the unit for the single-ridge serpentine waveguide, and Fig. 2(b)-(c) show the simulation results of different r_1 and r_2 for the unit, respectively. The voltage standing wave ratio (VSWR) is very sensitive to r_1 and r_2, and thus small changes of the radii will have a remarkable influence. We can see that r_1 mainly effects the low frequency performance of VSWR [Fig. 2(b)], while r_2 mainly the high frequency [Fig. 2(c)]. For balance, the r_1 and r_2 are chosen as 1.0 mm and 5.4 mm, respectively. Thus a very low VSWR(< 1.1) for the single ridge serpentine waveguide has been obtained.

To obtain good performance, it is important to design the slow-wave structure well, for it also determines the frequency bandwidth, the range of scanning angles, the loss of the antenna, etc. The inset in Fig. 1(a) shows the cross section of the serpentine waveguide, whose width and height are a and b, respectively. The ridge's width and height are s and $b - d$. The phase and frequency scanning angles are mainly determined by the width (a) and height (b) of the waveguide, respectively [26]. The phase scanning angle satisfies:

$$|\theta_p| \leq \arcsin\left(\frac{\lambda_0}{a+2t} - 1\right). \tag{1}$$

The frequency scanning angle satisfies:

$$|\theta_f| \leq \arcsin\left(\frac{\lambda_0}{d_s} - 1\right), \tag{2}$$

where

$$d_s = 2b + t + 2r_1 + w. \tag{3}$$

And the loss of the waveguide is mainly determined by both the width (s) and height ($b - d$) of the ridge. To avoid the grating lobes during phase scanning, the single-ridge waveguide instead of the standard rectangular waveguide is used to get a smaller element spacing $a + 2t$. As we can see, since individual characteristics are usually controlled by many parameters, it's difficult to separate them apart. The relations between the parameters and the performance of the array are listed detailedly in Table1. Therefore we should consider all of the relations above before designing the arrays.

TABLE 1. Parameters of dual-slot-waveguide array.

Performance	Relevant Parameters (mm).
Elevation scan angle	$a = 14,\ t = 1$
Azimuth scan angle	$b = 6,\ r_1 = 1,\ r_2 = 5.4,\ t = 1$
Slot resonant	$a = 14,\ b = 6,\ s = 3.75,\ d = 1.8$
Radiation power	$a = 14,\ b = 6,\ s = 3.75,\ d = 1.8$
VSWR	$b = 6,\ d = 1.8,\ r_1 = 1,\ r_2 = 5.4$
Loss	$b = 6,\ d = 1.8,\ r_1 = 1,\ r_2 = 5.4$

This article has been accepted for publication in a future issue of this journal, but has not been fully edited. Content may change prior to final publication. Citation information: DOI 10.1109/ACCESS.2020.2989318, IEEE Access

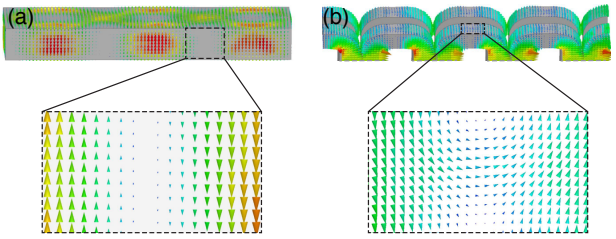

FIGURE 3. Current distributions of (a) the narrow wall of a rectangular waveguide and (b) the side chamber of a single-ridge waveguide.

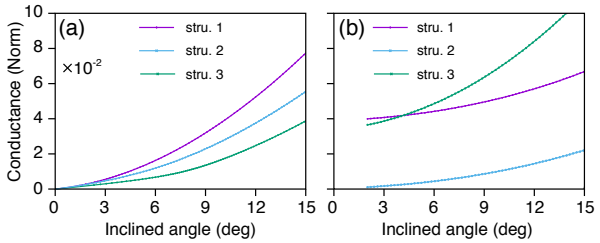

FIGURE 4. Normalized equivalent conductor. (a) Narrow-wall slotted rectangular waveguides with three different heights. (b) Side-chamber slotted single-ridge waveguides with three different ratios of b to d.

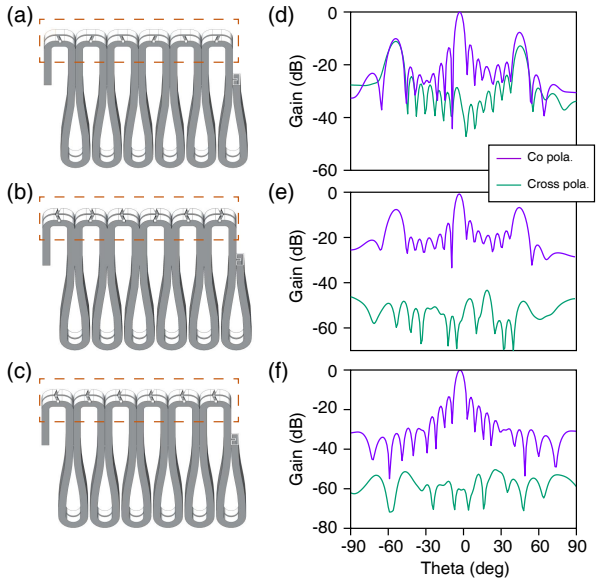

FIGURE 5. Schematic view of an SSDA with six dual slots and the corresponding radiation patterns. (a) Adjacent alternately mono slots array. (b) Adjacent alternately dual slots array. (c) Dual slots array with all the monomers inclined in same direction. (d)-(f) plot the corresponding radiation patterns for the structures shown in (a)-(c) .

It's worth noting that there is a main difference between the side-chamber dual slots and the narrow-wall inclined slots. As shown in Fig. 3(a), the current distribution of a rectangular waveguide, is completely transverse throughout the narrow wall; and that on the side chamber of a single-ridge waveguide, shown in Fig. 3(b), not only contains a transverse current, but also a lateral one throughout the chamber. When the slots are not inclined, the narrow-wall slot wouldn't radiate, and thus the equivalent conductor would be zero. However, the dual slots would remain on radiating because of the lateral currents. Fig. 4 shows the equivalent conductor of narrow-wall slot of rectangular waveguide and side-chamber slot of single-ridge waveguide for three different structures. We can see that for a narrow-wall slot, the equivalent conductor decreases as the inclined angle does, and tends to 0; but for the side-chamber slot, the conductor has a similar behavior as the narrow-wall one, except for tending to a nonzero value. These may provide some good insights towards designing waveguide slot antennas.

If low side-lobe level is required, structure of the serpentine waveguide must be carefully adjusted to get the minimal lateral current on the side chamber. Our study shows that the current distribution on the side chamber is mainly affected by the ratio of b to d. When the ratio becomes larger, the lateral current decreases; and the lateral current is negligible when it exceeds 4. Besides, in our design, the Taylor aperture distribution is used for the slot array synthesis by adjusting the inclined angles of the dual slots.

B. DUAL SLOTS

Waveguide slot antenna is a kind of aperture antenna, and the slots interrupt some of the wall current associated with the fundamental mode. This current interrupts induce an electric field distribution in the slot, which can be viewed as the radiation source. When radiating, the disturbed current on the wall of the waveguide will flow around the slots, thus the slots can be equivalent as the magnetic current sheets.

The dual slots, consisting of two opposite inclined slots located respectively on the side chambers, would be radiating by cutting the transverse currents. As illustrated in Fig. 1(b), monomers within the dual slots incline oppositely towards the perpendicular direction of the waveguide line. This exquisite design is to suppress the cross-polarization by radiation cancellation. The co-polarization, along the waveguide line, is enhanced by adding the horizontal electromagnetic field component of the dual slots together. While the cross-polarization, perpendicular to the waveguide line, is counteracted by the vertical field component of the dual slots. Furthermore, all the dual slots incline in same direction to suppress the unwanted high-mode radiation.

To show the merits of our dual-slot design, Fig. 5 gives three configurations of slot arrays and their corresponding radiation patterns. Among them, Fig. 5 (a) is a mono-slot array, Fig. 5 (b) and Fig. 5(c) are dual-slot arrays. The adjacent slots are arranged alternately in Fig. 5(a) and Fig. 5(b). While in Fig. 5(c), all the adjacent slots are inclined in same direction. The radiation patterns in Fig. 5(d)-Fig. 5(f) correspond respectively to Fig. 5(a)-Fig. 5(c).

Generally, adjacent alternately slots and oppositely inclined slots are used to reduce the cross-polarization of

This article has been accepted for publication in a future issue of this journal, but has not been fully edited. Content may change prior to final publication. Citation information: DOI 10.1109/ACCESS.2020.2989318, IEEE Access

the traveling wave slot array. As shown in Fig. 5(d), the adjacent alternately mono-slot array can reduce the cross-polarization about 10 dB, which would be the same as the co-polarization without alternated the adjacent slots. And the opposite inclined dual slots can reduce the cross-polarization about 40 dB. But for such waveguide structures, the adjacent alternately slot array will radiate the high-order radiations, leading to undesirable grating lobes; see Fig. 5(d) and (e). After considerable research, the dual slots, inclined in same direction, are chosen to be the radiating elements, as shown in Fig. 5(c). The radiation patterns in Fig. 5(f) show the best performance compared to two other. The array will have the same results when all the dual slots are inclined in the opposite direction to that in Fig. 5(c), because of the symmetry of the current distribution on the side-chamber of the structure.

C. ARRAY DESIGN

Fig. 6(a) gives an equivalent model of the single-ridge dual-slot-waveguide array with six dual slots. The single-ridge waveguide can be considered as a serpentine transmission line which transmits guided waves, and dual-slots are radiators coupling the fields inside the waveguide into free space. As seen in Fig. 6(a), the length of the slow-wave serpentine line and the distance between the two adjacent radiation elements are l and d_s, respectively. Then the interelement and space phase shifts can be expressed respectively as

$$\phi = \frac{2\pi}{\lambda_g} l, \tag{4}$$

$$\phi' = \frac{2\pi}{\lambda_0} d_s \sin\theta, \tag{5}$$

where λ_g is the guided wavelength in the serpentine guide, λ_0 the vacuum wavelength and θ the beam-scanning angle. When it satisfies

$$\phi - \phi' = 2m\pi, \tag{6}$$

we can substitute Eq. (4) and Eq. (5) into Eq. (6), and go straight to the beam-scanning angle

$$\begin{aligned} \theta &= \arcsin\left(\frac{l}{\lambda_g}\frac{\lambda_0}{d_s} - m\frac{\lambda_0}{d_s}\right) \\ &= \arcsin\left[\frac{1}{2\pi/\lambda_0}\left(\frac{2\pi}{\lambda_g}\frac{l}{d_s} - m\frac{2\pi}{d_s}\right)\right] \\ &= \arcsin\left(\frac{\beta'}{k_0}\right). \end{aligned} \tag{7}$$

Here $\beta' = [(2\pi l)/\lambda_g - 2m\pi]/d_s$ is the equivalent propagation constant in the slow-wave structure, and m is the rounded number of $\frac{l}{\lambda_g}$, deciding the frequency sensitivity.

The length of the meandering waveguide will be longer with the increase of integer number m. For a longer l, the interelement phase will change greater with the frequency, and the scanning angle of the structure will be more sensitivity to the frequency. But when the meandering waveguide becomes longer, the loss will be greater. So m is set to 4 to balance the sensitivity and loss. Fig. 7 plots the simulated

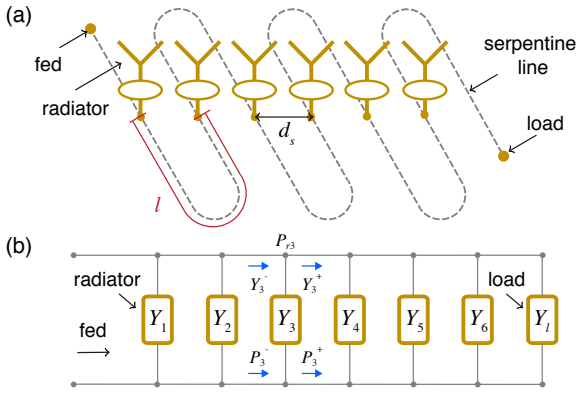

FIGURE 6. Equivalent model (a) and equivalent circuit (b) of the SSDA with six dual slots.

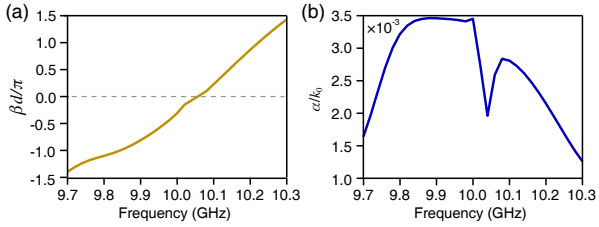

FIGURE 7. Dispersion diagram (a) and attenuation constant (b) versus frequency of the proposed SSDA.

dispersion diagram of the β' and the attenuation constant α versus frequency of the SSDA. Similar to the CRLH LWAs, the value of β' goes from negative to positive, indicating the backfire to endfire scan ability including the broadside direction. The attenuation constant is depressed around the resonant point, which is because of the coherent superposition of the reflection at the feed point. But the lowest value of α near the resonant point is not zero. Thus the open stop band of the structure is mitigated slightly, the structure can still radiate at the resonant point.

As seen in Fig. 6(b), it is an equivalent circuit of the dual-slot-waveguide array [27]–[29]. The dual-slot can be equivalent to a shunt admittance, thus we can use the circuit theory to obtain the dual-slots' admittance according to the Tayor aperture distribution. The meanings of the symbols in Fig. 6(b) are:

- $Y_i = G_i + jB_i$: The Normalized admittance of the i-th dual slots;
- $Y_i^+ = G_i^+ + jB_i^+$: The Normalized admittance seen from the right of the i-th dual slots to the load;
- $Y_i^- = G_i^- + jB_i^-$: The Normalized admittance seen from the left of the i-th dual slots to the load;
- P_{ri} : The power radiate by the i-th dual slots;
- P_i^+ : The power transmit from the right of the i-th dual slots to the load;
- P_i^- : The power transmit from the left of the i-th dual slots to the load.

This article has been accepted for publication in a future issue of this journal, but has not been fully edited. Content may change prior to final publication. Citation information: DOI 10.1109/ACCESS.2020.2989318, IEEE Access

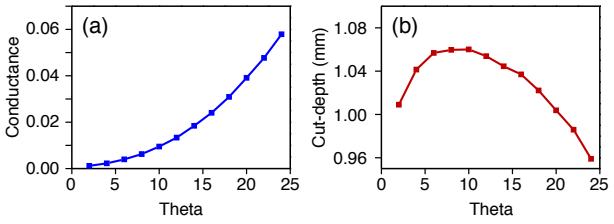

FIGURE 8. Fitting curves of initial values for array designing of (a) admittance (versus θ), (b) cut-depth (versus θ).

The dual slots can be thought of as working in the resonant case, hence the susceptance can be neglected. The admittance of the i-th dual slots can be written as:

$$G_i = \frac{P_{ri}}{P_i^+} G_i^+. \tag{8}$$

Because of the travelling wave situation and matched load, G_i^+ is approximate to 1. We need to obtain the value of P_i^+, if we want to get the G_i. According to the conservation of energy, we have:

$$\begin{aligned}
&P_1^+ = P - P_{r1},\\
&P_2^+ = qP_1^+ - p_{r2} = q(P - P_{r1} - P_{r2}q^{-1}),\\
&P_3^+ = qP_2^+ - p_{r3} = q^2\left(P - P_{r1} - P_{r2}q^{-1} - P_{r3}q^{-2}\right),\\
&\quad\vdots\\
&P_i^+ = q^{i-1}\left(P - \sum\nolimits_{j=1}^{i} P_{rj}q^{-j+1}\right),\\
&\quad\vdots\\
&P_N^+ = q^{N-1}\left(P - \sum\nolimits_{j=1}^{N} P_{rj}q^{-j+1}\right),
\end{aligned} \tag{9}$$

where q is the specific loss of the single ridge serpentine guide. P is the gross power that transmit to the SSDA. N is the total number of the slots. N is 6 in Fig. 6(b) for clarity. Combining Eq. (9) and Eq. (8, we can get:

$$Y_i = G_i = \frac{E_i^2 e^{-i+1}}{\frac{1}{\eta}\sum_{j=1}^{N} E_j^2 - \sum_{j=1}^{i} E_j^2 q^{-j+1}}, \tag{10}$$

where we use the following relations

$$P_{ri} \propto E_{ri}^2, \tag{11}$$

$$\eta = \frac{\sum_{j=1}^{N} P_{rj}}{P}. \tag{12}$$

Here E_{ri} is the aperture excitation coefficient, determined by the aperture distribution, and η is the antenna efficiency. Once the aperture distribution and antenna efficiency are selected, then the conductance of the dual slots can be determined accordingly. Meanwhile, we can use the simulation software to obtain the relation between the conductance and slot parameters (inclined angle θ and cut-depth d_c) by digging ten or more same dual slots into the SSDA to consider the slot coupling. Using the calculated conductance and fitting curves from the simulation results, we can determine the dual slots parameters. Fig. 8 shows the fitting curve of the relation between the conductance and the inclined angle, and that of the relation between the cut-depth and the inclined angle, respectively.

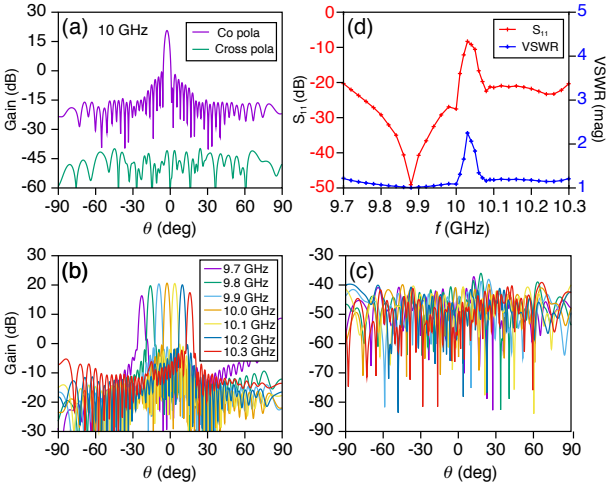

FIGURE 9. Simulated results of an SSDA. (a) Co- and cross-polarization radiation patterns at 10 GHz. (b)-(c) Radiation patterns of the 9.7-10.3 GHz band for co-polarization and cross-polarization respectively with frequency step 0.1 GHz. (d) Simulated S_{11} and VSWR with 0.01 GHz frequency step for resonance and 0.02 GHz for nonresonance.

III. ANALYSIS AND SIMULATION

Because of the long waveguide slow-wave line, the structure is complicated and electrically large. And thus it's time-consuming to simulate the whole two-dimensional scanned array. Therefore, in this paper, we just present the simulation results of an SSDA and three stacked SSDAs to validate the frequency-scanning and phase-scanning performance.

The design frequency and side lobe level of the SSDA are 10 GHz and -25 dB, respectively. The period of the dual slots in an SSDA is 21.2 mm, while that of SSDAs is 16 mm. As for the scanning angle, the array, actually several stacked SSDAs, can scan 45° along the waveguide in frequency and 120° perpendicular to the waveguide in phase without grating lobe.

A. SIMULATION RESULTS OF AN SSDA

In order to meet the aforementioned requirements, the parameters of the structure should be chosen carefully. After the parameter optimization, the width and height of the guide are chosen to be 14 mm and 6 mm, and those of the ridge to be 3.75 mm and 4.2 mm, repectively. In order to get fine frequency sensitivity, integer m is set to be 4. And we simulated 30 dual slots to validate the low sidelobe level. The slot width is 1.5 mm, and the detailed parameters of the slots are list in Table 2. The total length of an SSDA is about 0.7 m.

The simulation results of an SSDA are shown in Fig. 9, where (a) plots the co-polarization and cross-polarization

This article has been accepted for publication in a future issue of this journal, but has not been fully edited. Content may change prior to final publication. Citation information: DOI 10.1109/ACCESS.2020.2989318, IEEE Access

TABLE 2. Detailed parameters of the dual slots array.

No.	Distribution (Mag)	Conductor (Norm)	Inclined angle (deg)	Cut-depth (mm)
slots 1	0.69	0.0081	8.92	1.06
slots 2	0.70	0.0081	9.94	1.06
slots 3	0.72	0.0085	9.13	1.06
slots 4	0.75	0.0092	9.51	1.06
slots 5	0.80	0.0103	10.06	1.06
slots 6	0.85	0.0118	10.80	1.06
slots 7	0.91	0.0138	11.69	1.06
slots 8	0.98	0.0164	12.75	1.05
slots 9	1.05	0.0196	13.96	1.05
slots 10	1.11	0.0235	15.31	1.04
slots 11	1.17	0.0282	16.80	1.03
slots 12	1.23	0.0337	18.43	1.02
slots 13	1.27	0.0401	20.18	1.00
slots 14	1.30	0.0474	22.04	0.98
slots 15	1.31	0.0558	24.01	0.96
slots 16	1.31	0.0651	26.07	0.94
slots 17	1.30	0.0752	28.19	0.92
slots 18	1.27	0.0858	30.31	0.90
slots 19	1.23	0.0965	32.36	0.89
slots 20	1.17	0.1063	34.18	0.88
slots 21	1.11	0.1137	35.51	0.88
slots 22	1.05	0.1167	36.06	0.88
slots 23	0.98	0.1146	35.68	0.88
slots 24	0.91	0.1083	34.53	0.88
slots 25	0.85	0.0998	32.97	0.89
slots 26	0.80	0.0910	31.32	0.90
slots 27	0.75	0.0833	29.83	0.91
slots 28	0.72	0.0776	28.68	0.92
slots 29	0.70	0.0744	28.03	0.92
slots 30	0.69	0.0743	28.01	0.92

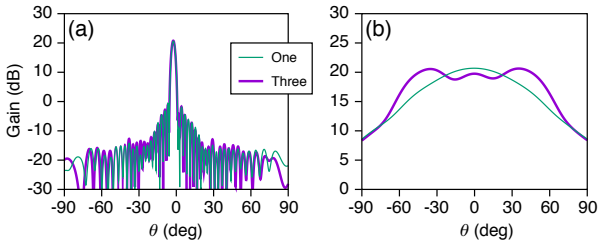

FIGURE 10. Simulation comparison between the radiation pattern of an SSDA alone and the active radiation pattern of the center SSDA within three stacked SSDAs for (a) E-plane and (b) H-plane.

radiation patterns at 10 GHz, respectively. We can see that the first sidelobe of the pattern (-1 dB) is about 21 dB lower than the main lobe (20 dB), and the cross polarization is below -40 dB. The radiation patterns of scanning frequency from 9.7 GHz to 10.3 GHz are shown in (b), covering $-23°$ to $16°$ in azimuth plane. As seen in (c), cross-polarization at different frequencies are all below -40 dB. The return loss S_{11} of the array is below -20 dB in the nonresonant working band and below -6 dB near resonant point, and the corresponding voltage standing wave ratio (VSWR) of the array shows the same behavior; see (d). Here the resonant point means that the inner spacing of the radiators is an integral multiple of the half guided wavelength. In this case, the backscattering of the radiators will interfere in phase at the feed port. This phenomenon will deteriorate the refection and gain.

B. SIMULATED ARRAY PERFORMANCE OF THREE STACKED SSDAS

In order to validate the array performance of the SSDA, we simulated the array consisting of three stacked SSDAs. The E-plane and H-plane radiation patterns of an SSDA and active pattern of the central subarray of three stacked SSDAs are shown respectively in Fig. 10. It can be seen from Fig. 10(a) that there is no difference between the E-plane radiation patterns. As a result, we can infer that adjacent SSDA doesn't have much influence on the performance of frequency scanning. As plotted in Fig. 10(b), the beam-width in H-plane of the central subarray of the stacked waveguide, about $120°$ with 4 dB gain drop, is wider than that of one waveguide. This indicates the maximum steering angle can be $\pm 60°$ in the plane perpendicular to the waveguide, leading to good array characteristics of such an SSDA.

IV. FABRICATION AND EXPERIMENTAL RESULTS

An sample of such SSDA is shown in Fig. 11, fabricated by CNC machining. Fig. 11(a) shows an oblique view of the SSDA, whose dimensions are 686 mm$\times$16 mm$\times$100 mm. Details of the dual slots are given in Fig. 11(b), where two opposite inclined slots are located on the two side chambers respectively. The coaxial-to-waveguide junction, a fourth-order Chebyshev impedance adapter here, is shown in Fig. 11(c) with the cover board removed to show the internal

This article has been accepted for publication in a future issue of this journal, but has not been fully edited. Content may change prior to final publication. Citation information: DOI 10.1109/ACCESS.2020.2989318, IEEE Access

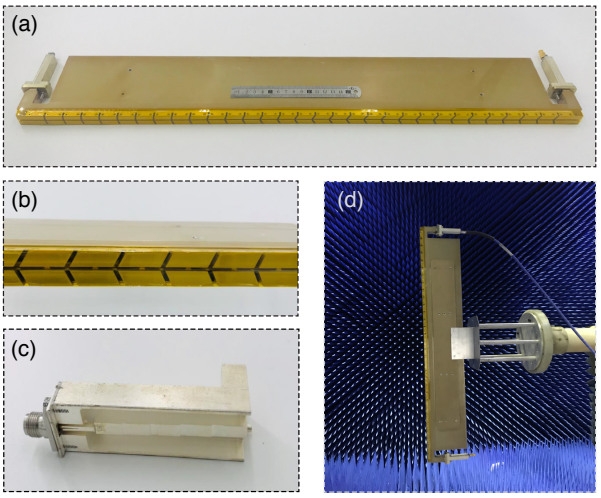

FIGURE 11. (a) Fabricated sample of an SSDA with a ruler (in centimeters) atop. (b) Enlarged view of the sample. (c) Coaxial-to-waveguide junction: a fourth-order Chebyshev impedance adapter. (d) Experimental setup for measurements.

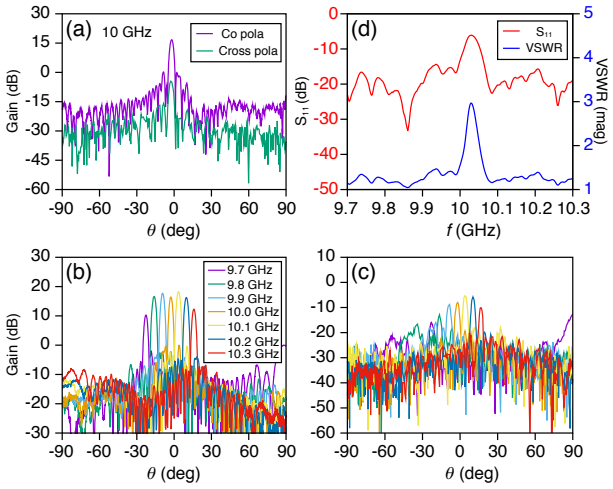

FIGURE 12. Measured results of an SSDA, corresponds to the simulated results in Fig. 9, respectively.

structure. The measurement and implementation setup of the SSDA is shown in Fig. 11(d). What should be pointed out is that in the fabricated structure, we didn't mill off the excess metal (Al) outside the serpentine line to reduce the processing time, making the sample look quite different from the schematics. The hollow serpentine waveguide is actually on the inside.

Far-field patterns of the SSDA are measured in a compact anechoic chamber. Thus it's kind of difficult to align the detector with the main beam of the SSDA, specifically about 2.5° width in E-plane. Fig. 12(a) plots the measured radiation patterns for both co- and cross-polarizations at 10 GHz. It's measured that the first sidelobe of the pattern (-0 dB) is about 18 dB lower than the main lobe (18 dB), and the cross-polarization is below -25 dB, which

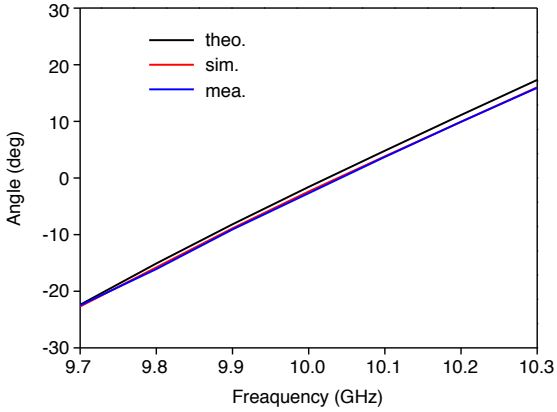

FIGURE 13. Theoretical, simulated and measured main beam angles of the designed SSDA.

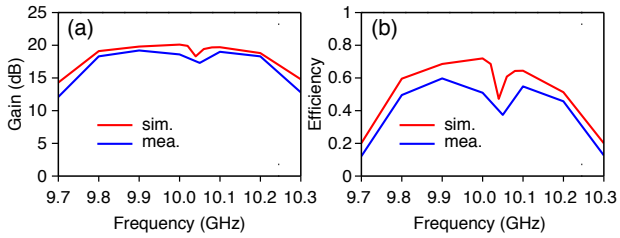

FIGURE 14. Measured and simulated realized gains and radiation efficiencies of the designed SSDA.

have subtle differences with the simulations as shown in Fig. 9(a). The sidelobe difference stems from the scattering errors in the measurement environment. And a higher cross-polarization over the band is mainly due to processing errors, making the dual-slot monomer asymmetric. Since high cross-polarization of the array is completely eliminated when the oppositely inclined dual-slot monomers are machined perfectly, thus it's quite sensitive to symmetry of the dual-slot configuration. Fig. 12(b) and (c) give the measured co- and cross-polarization patterns over the 9.7-10.3 GHz band. Except for some inevitable deviations in gain, the measured main beams coincide well with the simulated ones shown in Fig. 9. Measured VSWR of the sample is shown in Fig. 12(d), where the whole profile agrees well with the simulation. Here, the main difference that small ripples occur is due to the different frequency steps between measurement and simulation.

The measured main beam angles of the designed SSDA are plotted in Fig. 13, which agrees well with the theoretical predictions and the simulation results. Beam-steering range from $-23°$ to $+16°$ is realized when the frequency scans from 9.7 GHz to 10.3 GHz, which indicates the high frequency sensitivity of 65°/GHz. Fig. 14 shows the realized gain and radiation efficiency of this frequency scanning SSDA. As seen in Fig. 14(a), the measured maximum gain is 19 dB. The maximum discrepancy between the simulated and measured gains is 2 dB. That is due to machining and welding errors,

TABLE 3. Performance comparisons with existing FSAs.

Ref.	Antenna Type	Size $L \times W \times H(\lambda_0)$	Freq. Range GHz	Scanning Range deg	Freq. Sensitivity deg/GHz	Gain dB	SLL dB	Cross Pol. dB
[8]	Slow-wave waveguide	$11.9 \times 3.6 \times 0.75$	$6.6 - 6.9$	$+52° \sim +85°$	80	13.1	-10	N/A
[12]	Slow-wave microstrip	$8.7 \times 1.5 \times 0.17$	$8.9 - 10.6$	$-27.5° \sim +46°$	43.24	15.5	-20	N/A
[15]	Microstrip LWA	$3.76 \times 0.9 \times 0.05$	$23.8 - 24.2$	N/A	N/A	10	-10	-15
[17]	SIW based LWA	$9.3 \times 0.37 \times 0.03$	$13.5 - 16.5$	$-30° \sim +30°$	20	10	-11.4	-20
[18]	CRLH SIW	$2.64 \times 0.42 \times 0.05$	$24 - 27$	$-17° \sim +13°$	10	13.2	-22	-15
[20]	CRLH waveguide	$34 \times 0.53 \times 0.9$	$32.8 - 40$	$-20° \sim +31°$	7.08	19.6	-18.5	N/A
[25]	RWG slot	$11.9 \times 7 \times 0.34$	$24.5 - 26.5$	$+1° \sim +14°$	6.5	13	-5	-14
This Work	SSDA	$22.8 \times 0.53 \times 3.3$	$9.7 - 10.3$	$-23° \sim +16°$	65	20	-21	-45

which makes the loss of the actual structure higher than ideal one. The measured gain is more than 12 dB within the whole frequency range. The measured maximum efficiency is about 60%, as shown in Fig. 14(b). The notches in the gain curve and the radiation efficiency curve are in accordance with the aforementioned resonance phenomenon. What can be noted, however, is that the radiation efficiency at both ends of the frequency band is a little lower. The low efficiency of the band ends is because of the narrow resonance bandwidth of the slots. Therefore, most of the energy is absorbed by the terminated load. The long slow-wave structure and the low sidelobe aperture distribution are also the factors leading to this situation. Fortunately, designers have the flexibility to adjust the sidelobe level, frequency sensitivity and transmission losses of the proposed slow-wave waveguide by choosing proper m and number of slots.

Features of this paper are compared with other references in Table 3. It is clear that the proposed frequency scanning SSDA has high frequency sensitivity, low cross-polarization, low sidelobe level, as well as acceptable scanning range and antenna size. Moreover, the SSDA is advantageous in terms of good stability and reliability, long life and high power handling capability. However, it should be pointed out that the profile of our structure (H) is a little higher than the planar arrays. This is due to the use of meandering slow-wave structure in the height direction. Thus our structure is suitable for specific outdoor applications, which value good stability and reliability, and high power handling capability more than compact size.

V. CONCLUSION

A frequency scanning dual-slot-waveguide array is studied in this paper. For an SSDA, it scans from the backfire to the endfire in a narrow bandwidth resource with a frequency sensitivity of 65°/GHz. A -21 dB or even lower first sidelobe is obtained. The cross-polarization is also kept at a very low value (-45 dB) or much lower. As for three stacked SSDAs, it realize a 120° phase-scanning, with no influence on the frequency-scanning of the individual 1D subarray. Compared to the conventional 2D phased arrays, our frequency-scanning waveguide-line structure uses much less phase shifters. It is much simpler and cheaper so that it will have a broad application in civilian fields. Last but not least, it should be pointed out that the array still suffers from the common problem in periodic LWAs, that when the inner spacing of the radiators is an integral multiple of the half wavelength (called resonant point), the backscattering of such radiators will interfere constructively at the feed port. This phenomenon would deteriorate the reflection, leading to a peak in S_{11} curve (about -6 dB in our structure). In the future work, we could use random dual-slots and add reflection-cancelling structure to break constructive interference, thus reducing the return loss at the resonant point.

REFERENCES

[1] R. Mailloux, "Phased array antenna handbook," 2nd ed., Norwood, LD, UK: Artech House, pp. 600–613, 2005.
[2] J. N. Zhong, A. Johnson, E. A. Alwan, and J. L. Volakis, "Dual-Linear Polarized Phased Array With 9 : 1 Bandwidth and 60° Scanning Off Broadside," IEEE Transactions on Antennas and Propagation, vol. 67, no. 3, pp. 1996–2001, 2019.
[3] E. W. Reid, L. Ortiz-Balbuena, A. Ghadiri, and K. Moez, "A 324-element Vivaldi antenna array for radio astronomy instrumentation," IEEE Transactions on Instrumentation and Measurement, vol. 61, no. 1, pp. 241–250, 2011.
[4] A. Ishimaru and H. S. Tuan, "Theory of frequency scanning of antennas," IRE Transactions on Antennas and Propagation, vol. 10, no. 2, pp. 144–150, 1962.
[5] A. F. Zhang, R. Yang, D. Ling, B. W. Hu, Z. Y. Lei, and Y. C. Jiao, "Metasurface-based tapered waveguide slot array antennas for wide angular scanning in a narrow frequency band," IEEE Transactions on Antennas and Propagation, vol. 66, no. 8, pp. 4052–4059, 2018.
[6] A. A. Oliner, D. R. Jackson, and J. L. Volakis, "Antenna engineering handbook," New York, NY, USA: McGraw-Hill, 2007.
[7] J. Hilburn, and F. Prestwood, "K band frequency-scanned waveguide array," IEEE Transactions on Antennas and Propagation, vol. 22, no. 2, pp. 340–342, 1974.
[8] E. Hamidi, "Design, analysis and simualtion of a C band frequency scanning slot-array antenna," International Conference on Computer and Communication Engineering (ICCCE'10), pp. 1–5, 2010.
[9] H. Wang, y. D. Zhang, Y. Wang, S. L. Quan, and D. L. Xu, "Low-loss frequency scanning planar array with hybrid feeding structure for low-altitude detection radar," The Journal of Engineering, vol. 2019, no. 20, pp. 6708–6711, 2019.
[10] R. S. Elliot, "Antenna Theory and Design," 1st ed., D. G. Dudley, Ed. Hoboken, NJ, USA: Wiley: Wiley, 2003.
[11] M. Danielsen, and R. Jorgensen, "Frequency scanning microstrip antennas," IEEE Transactions on Antennas and Propagation, vol. 27, no. 2, pp. 146–150, 1979.
[12] L. Cui, W. Wu, and D. G. Fang, "Printed frequency beam-scanning antenna with flat gain and low sidelobe levels," IEEE Antennas and Wireless Propagation Letters, vol. 12, pp. 292–295, 2013.
[13] C. Vazquez, C. Carcia, Y. Alvarez, S. Ver-Hoeye, and F. Las-Heras, "Near field characterization of an imaging system based on a frequency scanning antenna array," IEEE Transactions on Antennas and Propagation, vol. 61, no. 5, pp. 2874–2879, 2013.

[14] Y. J. Cheng, W. Hong, K. Wu and Y. Fan, "Millimeter-Wave Substrate Integrated Waveguide Long Slot Leaky-Wave Antennas and Two-Dimensional Multibeam Applications," IEEE Transactions on Antennas and Propagation, vol. 59, no. 1, pp. 40-47, 2011.

[15] A. Al-Bassam, S. Otto, D. Heberling, and C. Caloz, "Broadside dual-channel orthogonal-polarization radiation using a double-asymmetric periodic leaky-wave antenna," IEEE Transactions on Antennas and Propagation, vol. 65, no. 6, pp. 2855–2864, 2017.

[16] A. Zhang, R. Yang, D. Li, B. Hu, Z. Lei and Y. Jiao, "Metasurface-Based Tapered Waveguide Slot Array Antennas for Wide Angular Scanning in a Narrow Frequency Band," IEEE Transactions on Antennas and Propagation, vol. 66, no. 8, pp. 4052-4059, 2018.

[17] S. Rezaee, and M. Memarian, "Analytical Study of Open-Stopband Suppression in Leaky-Wave Antennas," IEEE Antennas and Wireless Propagation Letters, vol. 19, no. 2, pp. 363–367, 2020.

[18] W. Q. Cao, Z. N. Chen, W. Hong, B. N. Zhang, and A. J. Liu, "A beam scanning leaky-wave slot antenna with enhanced scanning angle range and flat gain characteristic using composite phase-shifting transmission line," IEEE Transactions on Antennas and Propagation, vol. 62, no. 11, pp. 5871–5875, 2014.

[19] M. Alibakhshikenari, B. S. Virdee, M. Khalily, P. Shukla, C. H. See, R. Abd-Alhameed, F. Falcone, and E. Limiti, "Beam-scanning leaky-wave antenna based on CRLH-metamaterial for millimetre-wave applications," IET microwaves, antennas & propagation, vol. 13, no. 8, pp. 1129–1133, 2019.

[20] Q. S. Yang, X. W. Zhao, and Y. H. Zhang, "Design of CRLH leaky-wave antenna with low sidelobe level," IEEE Access, vol. 7, pp. 178224–178234, 2019.

[21] C. A. Balanis, "Modern Antenna Handbook," 1st ed., Hoboken, NJ, USA: Wiley, 2008.

[22] Per-Simon. Kildal, E. Alfonso, A. Valero-Nogueira, and E. Rajo-Iglesias, "Local metamaterial-based waveguides in gaps between parallel metal plates," IEEE Antennas and Wireless Propagation Letters, vol. 8, pp. 84–87, 2008.

[23] S. A. Razavi, P. Kildal, L. Xiang, E. Alfonso Alós and H. Chen, "2× 2-slot element for 60-GHz planar array antenna realized on two doubled-sided PCBs using SIW cavity and EBG-type soft surface fed by microstrip-ridge gap waveguide," IEEE Transactions on Antennas and Propagation, vol. 62, no. 9, pp. 4564–4573, 2014.

[24] M. Al sharkawy, and A. A. kishk, "Long slots array antenna based on ridge gap waveguide technology," IEEE Transactions on Antennas and Propagation, vol. 62, no. 10, pp. 5399–5403, 2014.

[25] M. Al sharkawy, and A. A. kishk, "Split slots array for grating lobe suppression in ridge gap guide,"IEEE Antennas and Wireless Propagation Letters, vol. 15, pp. 946–949, 2015.

[26] T. S. Chen, "Calculation of the parameters of ridge waveguides," IRE Transactions on Microwave Theory and Techniques, vol. 5, no. 1, pp. 12–17, 1957.

[27] H.T. Zhang, W. Wang, Z.H. Zhang, and X.J. Ma, "A novel dual-polarized waveguide antenna with low cross-polarization for sar applications," Microwave and Millimeter Wave Technology (ICMMT), 2012 International Conference, vol. 3, pp. 1–3, 2012.

[28] B. Das, J. Ramakrishna, and B. Sarap, "Resonant conductance of inclined slots in the narrow wall of a rectangular waveguide," IEEE transactions on antennas and propagation, vol. 32, no. 7, pp. 759–761, 1984.

[29] W. S. Yin, "Wide-band and wide-angle array antenna,"Ph.D. dissertation, Fudan Univ., ShangHai, SH, PRC, 2019

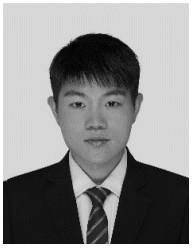

WEISHUANG YIN was born in Xiantao, Hubei, China. He received the B.S degree in physical science and technology from LanZhou University, in 2014 and the Ph.D degree in condensed matter physics from Fudan University, in 2020.

His research interests include waveguide slot array antenna, patch array antenna, ultra-wideband array antenna and artificial bandgap material.

ANG CHEN was born in Puyang, Henan, China in 1990. He received the B.S degree in applied physics from Tongji University, in 2012 and the Ph.D degree in condensed matter physics from Fudan University, in 2018.

From 2018 to 2019, he was a Research Assistant in Department of Electrical and Computer Engineering, University of Wisconsin-Madison, USA, mainly working on the artificial intelligence (AI), and also on nanophotonics. Since 2019, he was a System Engineer in Ideaoptics Inc., Shanghai, China. His research interests include nanophotonics, image processing and optical critical dimension for structure metrology, investigating by the method of deep neural networks.

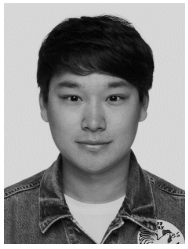

XIUYE LIANG was born in Handan, Hebei, China, in 1993. He received the B.S. degree in optoelectronic information science and engineering from Jiangnan University, Wuxi, China, in 2016.

He is currently pursuing the Ph.D. degree in Fudan University, Shanghai, China. His current research interests include phased array feed antennas, UWB antenna arrays, artificial bandgap materials, and artificial intelligence in antenn design.

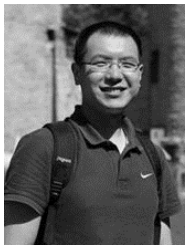

LEI SHI received the B.S. degree in bio-physics from Nanjing University, Jiangsu, China, in 2005 and the PhD. degree in condense matter physics from Fudan University, Shanghai, China, in 2010. From 2011 to 2013, he was a post-doctoral researcher in CSIC-ICMM/UPV, Spain and Aalto University, Finland.

He is currently a professor in department of physics at Fudan University, Shanghai, China. His research interest includes photonic crystals, micro- and nano- photonic materials and the development of advanced optical characterization techniques.

Prof. Shi's awards and honors include the Shanghai Outstanding Technical Leaders (Shanghai Municipal Science and Technology Commission, 2019), Eastern Scholar Distinguished Professors (Shanghai Municipal Education Commission, 2014).

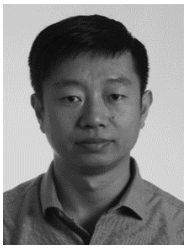

FANG GUAN was born in Yixian, Liaoning Province, China, in 1979. He received the B.S. degree in applied physics from Fudan University, China, in 2002, and the M.S. and Ph.D. degrees in condensed matter physics from Fudan University, in 2005 and 2014, respectively.

From 2014 to 2019, he was a Research Assistant working in Physics Department of Fudan University. Currently, he is an Associated Professor in the Institute for Nanoelectronic Devices and Quantum Computing of Fudan University. His research interests include Photonic crystals, metasurfaces, phased arrays and ultrawideband antenna arrays.

XIAOHAN LIU was born in Jiangsu, China. He received the B.S, Master and Ph.D degrees in Fudan University in 1993, 1996 and 1999, respectively.

From 2003 to 2007, he was a Lecturer with the department of physics, Fudan University, and the post-doctor in university of Munster, Germany. From 2007 to 2012, he was a associate professor with the department of physics, Fudan University. Since 2012, he has been a professor with the department of physics, Fudan University. He has authored or coauthored over 100 technical papers. His current research interests include Optical properties of condensed matter, Photonic crystals and array antenna.

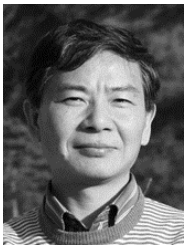

JIAN ZI was born in Sichuan, China. He received the B.S, Master and Ph.D degrees in Fudan University in 1985, 1988 and 1991, respectively.

From 1991 to 1995, he was a Lecturer with the department of physics, Fudan University, and the post-doctor in university of Munster, Germany. From 1994 to 1995, he was a associate professor with the department of physics, Fudan University. Since 1996, he has been a professor with the department of physics, Fudan University, and access to the National Science Fund for Distinguished Young Scholars. He has been a Chang-Jiang Profosor nominated by the Ministry of Education of China, since 2001. He was appointed as the chief scientist of project 973 by the Ministry of Science and Technology in 2001 and 2007. He has authored or coauthored over 300 technical papers. His current research interests include Photonic crystals, plasmonics, metamaterials, natural photonic structures and structural colors, liquid surface waves propagating in periodic structures.